

# Electron-hole capture kinetics in luminescent conjugated polymers

Stoyan Karabunarliev and Eric R. Bittner\*

Department of Chemistry, University of Houston, Houston, TX 77204-5003

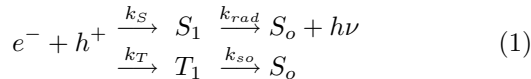
(Dated: December 2, 2024)

Electron-hole (e-h) capture in luminescent conjugated polymers (LCPs) is modeled by the dissipative dynamics of a multilevel electronic system coupled to a phonon bath. Electroinjected e-h pairs are simulated by a mixed quantum state, which relaxes via phonon-driven internal conversions to low-lying charge-transfer (CT) and excitonic (XT) states. The underlying two-band polymer model reflects PPV and spans monoexcited configuration interaction singlets (S) and triplets (T), coupled to Franck-Condon active C=C stretches and ring-torsions. Focusing entirely upon long PPV chains, we consider the recombination kinetics of an initially separated CT pair and address the issue electroluminescent enhancement in organic light-emitting diode materials. Our model calculations indicated that S and T recombination proceeds according to a branched, two-step mechanism dictated by near e-h symmetry. The initial relaxation occurs rapidly with nearly half of the population going into excitons ( $S_{XT}$  or  $T_{XT}$ ), while the remaining portion remains locked in metastable CT states. While formation rates of  $S_{CT}$  and  $T_{CT}$  are nearly equal,  $S_{XT}$  is formed about twice as fast  $T_{XT}$  in concurrence with experimental observations of these systems. Furthermore, breaking e-h symmetry suppresses the XT to CT branching ratio for triplets and opens a slow CT  $\rightarrow$  XT conversion channel exclusively for singlets due to dipole-dipole interactions between geminate and non-geminate configurations. Finally, our calculations yield a remarkable linear relation between chain length and singlet/triplet branching ratio which can be explained in terms of the binding energies of the respective final excitonic states.

## I. INTRODUCTION

Since the discovery of electroluminescence (EL) in poly(p-phenylene vinylene) PPV,<sup>1</sup> considerable efforts have gone in development and commercialization of light-emitting diodes (LEDs), based on luminescent conjugated polymers (LCPs). While much progress has been made in improving emission efficiency and color control,<sup>2</sup> the detailed physics of charge transport and light generation in these materials is relatively poorly understood in comparison with inorganic semiconductors. The one-dimensional delocalization of electrons and substantial electron-hole and electron-lattice interactions render the delineation of neutral and charged excitations in LCPs very complex and demanding. Moreover, a dynamical description is needed in order to capture the transient relaxation processes that occur when charged species approach each other, recombine and decay.

Photogenerated singlet e-h pairs in LCPs typically relax to highly emissive  $S_1$  excitons prior to decay. In contrast, electroinjected electrons ( $e^-$ ) and holes ( $h^+$ ) are not spin correlated and can combine to form both singlet and triplet excitons.



Because the decay of the triplet exciton  $T_1$  is nearly radiationless and relaxation to  $S_0$  occurs via spin-orbit coupling, quantum efficiency in electroluminescence ( $\eta_{EL}$ ) is only a fraction of that for photoluminescence ( $\eta_{PL}$ ). If the rate of e-h capture is spin-independent,  $S_1$  and  $T_1$  excitons are formed in a 1:3 ratio as dictated by spin degeneracy. In such a case, 75% of the bound e-h pairs are non-emissive leading to a theoretical max-

imum of  $\eta_{EL} = 0.25 \eta_{PL}$ . Nonetheless, efficiencies of up to  $\eta_{EL} = 0.50 \eta_{PL}$  have been achieved independently on PPV-based LEDs in the laboratories of Heeger<sup>2</sup> and Friend<sup>3,4</sup>. From this it has been inferred that in organic light-emitting polymers, singlet  $e-h$  capture is intrinsically more efficient than the respective triplet process ( $k_S > k_T$ ).

If we assume that the formation kinetics is first order such that the singlet and triplet exciton population formation rates are proportional to the total population of charge-transfer (CT) states in the system, then the formation cross-section  $\sigma_s$  for singlet excitons as given by the ratio of singlets to total excitons by

$$\sigma_s = \frac{N_s(t)}{N_s(t) + 3N_T(t)} = \frac{r}{r + 3} \quad (2)$$

where  $r = k_S/k_T = \sigma_S/\sigma_T$ . In order to obtain the nearly 64% EL efficiencies reported by various groups<sup>2,3</sup> in various organic polymer LED devices,  $r$  must be in the range of  $3 < r < 5$ . Such ratios were also obtained for a wide range of organic LCPs via PADMR experiments by Wohlgenannt, *et al.*<sup>7,8</sup> which measures the population of photo-generated intrachain parallel and anti-parallel polaron pairs in the presence of a magnetic field.

Various mechanisms favoring the formation of  $S_1$  versus  $T_1$  have been proposed for both interchain and intrachain e-h collisions. Using Fermi's golden rule, Shuai, Bredas *et al.*<sup>9,10</sup> indicate that the  $S$  cross section for interchain recombination can be higher than the triplet one due to bond-charge correlations. Wohlgenannt *et al.*<sup>7</sup> resort to a similar model of two parallel polyene chains. Both of these works neglect vibronic and relaxation effects. In simulating the intrachain collision of opposite polarons, Kobrak and Bittner<sup>11,12</sup> show that formation

of  $S_1$  is enhanced by the near-resonance with the free e-h pair. The result reflects the fact that spin-exchange renders  $T_1$  more tightly bound than  $S_1$ ,<sup>13</sup> and hence more electronic energy must be dissipated in the formation of the former. The energy-conservation constraints in spin-dependent e-h recombination have been analyzed by Burin and Ratner<sup>14</sup> in an essential-state model. The authors point out that nonradiative processes (internal conversion, intersystem crossing) must entail C=C stretching vibrons since these modes couple most strongly to  $\pi \rightarrow \pi^*$  excitations.

In this work, we describe e-h capture in LCPs in terms of the dissipative dynamics of a multi-level electronic system coupled to a phonon bath. Our model is based upon a two-band polymer model introduced by Soos, Mazumdar, *et al*<sup>15</sup> augmented by the coupling of electronic excitations to a bath of vibrational modes. First, we develop a concise and predictive model for simulating via quantum chemical methods the transient relaxation dynamics of an excited state in an extended system. The methodology we develop herein is applicable to both excitonic transfer (i.e. Förster) as well as charge-transfer states in a general conjugated polymer system. At the present, we restrict our attention to mono-excited closed-shell systems; however, the approach can be extended to the general case for radicals. Secondly, we examine a specific physical process involving the collision and relaxation of injected electron-hole pairs in luminescent conjugated polymers, such as PPV. Our calculations underscore the role that vibronic coupling and electron-hole symmetry play in determining the singlet-triplet branching ratio as the CT state relaxes to form bound electron/hole excitonic pairs. Finally, we explore the relation between chain length and the singlet/triple branching ratio. We show that our methodology reproduces the remarkably universal linear relation between conjugation length and  $r$  as evident in a wide range of conjugated polymer materials. To our knowledge, ours is the first molecular based model which accurately predicts this linear relation for a specific molecular system and provides a rationalization for this trend based upon the variation of the exchange energy with increasing chain length.

## II. METHODOLOGY

### A. Two-band polymer model + phonons

The Hamiltonian for the coupled system is

$$\begin{aligned}
H &= H_{el} + H_{ph} + H_{el-ph} \\
&= \sum_{mn} (F_{mn}^o |m\rangle \langle n|) \\
&\quad + \frac{1}{2} \sum_{\mu\nu} \kappa_{\mu-\nu} q_\mu q_\nu + \delta_{\mu\nu} p_\mu^2 \\
&\quad + \sum_{mn\mu} \left( \frac{\partial F_{mn}}{\partial q_\mu} \right)_o q_\mu |m\rangle \langle n| \quad (3)
\end{aligned}$$

The electronic Hamiltonian  $H_{el}$  represents the configuration interaction of localized singlet of triplet configurations  $|m\rangle = |\overline{m}m\rangle$  with a valance hole in repeat unit  $\overline{m}$  and a conduction electron in repeat unit  $m$ . For example, the  $|\overline{m}m\rangle$  geminate monoexcited configuration for a 5 repeat-unit system is

$$|\overline{m}m\rangle = \left( \begin{array}{ccccc} \bar{\downarrow} & \bar{\downarrow} & \uparrow & \bar{\downarrow} & \bar{\downarrow} \\ \downarrow & \downarrow & \downarrow & \downarrow & \downarrow \end{array} \right) \quad (4)$$

where as

$$|\overline{m}n\rangle = \left( \begin{array}{ccccc} \bar{\downarrow} & \bar{\downarrow} & \bar{\downarrow} & \bar{\downarrow} & \uparrow \\ \downarrow & \downarrow & \downarrow & \downarrow & \downarrow \end{array} \right) \quad (5)$$

represents a charge-transfer state.

System specific information is incorporated by using valance and conduction band Wannier functions (WF)  $|\overline{m}\rangle$  and  $|m\rangle$  as the single particle basis. For the single-particle band-structure we use a Hartree-Forck Pariser-Parr-Pople (PPP) approximation which can be parameterized easily for a variety of luminescent conjugated polymer systems. and construct maximally optimized Wannier functions. The single-particle terms,  $F_{mn}^o$ , are derived at the ground state equilibrium configuration,  $q_\mu = 0$ , from the Fourier components  $f_r^o$  and  $\overline{f}_r^o$  of the band energies in pseudomomentum space.

$$\begin{aligned}
F_{mn}^o &= \delta_{\overline{m}n} \langle m | f^o | n \rangle - \delta_{mn} \langle \overline{m} | \overline{f}^o | \overline{n} \rangle \\
&= \delta_{\overline{m}n} f_{m-n}^o - \delta_{mn} \overline{f}_{\overline{m}-\overline{n}}^o \quad (6)
\end{aligned}$$

For extended  $\pi$ -systems with electron-hole symmetry, the localized electron/hole energy levels and transfer parameters are related by  $\overline{f}_r = -f_r$  and reflect the cosine-shaped valance and conduction bands of half-width  $f_1^o$  and centered at  $\pm f_o^o$  respectively.

The two-particle interactions are spin dependent with

$$\begin{aligned}
V_{mn}^T &= -\langle m\overline{n} | |n\overline{m}\rangle \quad (7) \\
V_{mn}^S &= V_{mn}^T + 2\langle m\overline{n} | |m\overline{n}\rangle. \quad (8)
\end{aligned}$$

with

$$\langle m\overline{n} | |i\overline{j}\rangle = \int d1 \int d2 \phi_m(1)^* \phi_n^*(2) v(12) \phi_i(1) \phi_j(2)$$

With the exception of geminate WFs, orbital overlap is small such that the two-body interactions are limited to Coulomb and exchange integrals reflecting e-h attraction and spin-exchange coupling non-geminate configurations and transition dipole-dipole integrals coupling only geminate singlet electron-hole pairs. In the absence of e-h symmetry, dipole-dipole coupling between singlet geminate and non-geminate configurations is introduced through this term. As we shall explore later in this paper, this opens a channel for coupling singlet charge-transfer states to singlet excitonic states but does not allow for coupling between the triplet CT to XT states.

Finally, the electron-phonon coupling term,  $H_{el-ph}$  describes the local variation of the single-particle band gap

and is taken to be linear a set of phonon normal-mode coordinates  $q_\mu$  which are localized within a single unit-cell. The linear coupling strength for both the electron and holes,  $(\partial f/\partial q_\mu)_o = -(\partial \bar{f}/\partial q_\mu)_o$ , is adjusted empirically as to reproduce the vibronic progressions observed in the single-photon absorption and emission spectra. Correspondingly, the vibrational term,  $H_{ph}$  models weakly dispersed optical phonon branches in the frequency ranges of the dominant Franck-Condon active modes observed in the experimental spectra. For the case of PPV considered here, the phonon term consists of two sets of local harmonic oscillators with weak nearest-neighbor coupling, representing two dispersed optical phonon branches, centered at 1600 and 100 $\text{cm}^{-1}$ , respectively. These frequencies roughly correspond to C=C bond stretches and ring-torsional motions (librations), which dominate the Franck-Condon activity in PPV and related polymers.<sup>18</sup> Huang-Rhys factors (dimensionless el-ph coupling constants) for  $S_1$  of the isolated monomer were subsequently set to 0.8 for the high-frequency mode and 10 for the low-frequency mode.

## B. Diabatic Representation

Having set up the primitive Hamiltonian and parameterized it according to a model physical system, we can obtain the diabatic electronic/vibrational structure by separately diagonalizing  $H_{el}$  and  $H_{ph}$  yielding a series of vertical excited states with energies  $\varepsilon_a^o$  (from  $q_\mu = 0$ ) and a normal modes with frequencies  $\omega_x i$ . Written in the diabatic representation

$$\begin{aligned} \tilde{H} = & \sum_a \varepsilon_a^o |\mathbf{a}\rangle \langle \mathbf{a}| \\ & + \frac{1}{2} \sum_\xi (\omega_\xi^2 Q_\xi^2 + P_\xi^2) \\ & + \sum_{ab\xi} g_{ab\xi}^o Q_\xi |\mathbf{a}\rangle \langle \mathbf{b}|. \end{aligned} \quad (9)$$

The diabatic coupling term  $g_{ab\xi}^o$  is simply the original electron-phonon coupling tensor transformed into this new representation. The density of states (DOS) for vertical singlet and triplet excitations from the ground state for a PPV model with 32 repeat units ( $PPV_{32}$ ) is shown in Fig. 1, as parameterized from the  $\pi$ -band structure and Wannier functions of the extended polymer. Although the Stokes shifts from adiabatic relaxation of the excited states is missing in this calculation, the lowest singlet  $S_1$  and triplet  $T_1$  excitons differ significantly in terms of their binding energies. Here,  $T_1$  is roughly 1 eV lower than the  $S_1$  in general agreement with experimental and theoretical estimates.

We can also use the diabatic representation to calculate the relaxed excited states and their respective potential energy curves. This we achieve by variational minimization of the adiabatic energy  $\varepsilon_a = \langle \mathbf{a} | \tilde{H} | \mathbf{a} \rangle$  of each indi-

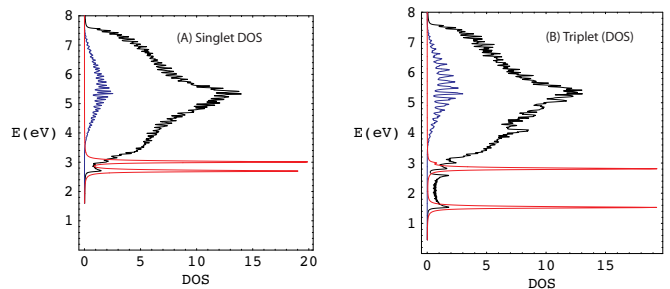


FIG. 1: Density and population of singlets (A) and triplets (B): density of states - black; initial population - blue; population at 100ps - red.

vidual state according to

$$\frac{\partial \varepsilon_a}{\partial Q_\xi} = g_{aa\xi} + \omega_\xi^2 Q_\xi = 0. \quad (10)$$

The relaxed excited states are eigenstates of  $\tilde{H}_{el} + \tilde{H}_{ph}$  at state specific conformations,  $Q_{\xi,a} \neq 0$ , displaced from the ground state at  $Q_\xi = 0$ . Such displacements modify the optical spectra by moving states into and out of regions of strong Franck-Condon coupling to the ground state.

Thus, we can test the parameterization of the model by computing the Condon spectral density for single photon absorption. The cumulative spectral density of  $PPV_{32}$  is given in Fig. 2 for both the vertical and Condon approximation. Individual electron-vibrational transitions are taken to give Lorentzian lineshapes of half-width 0.01eV. The oscillator strengths for the  $S_o \rightarrow S_a$  vertical transitions were computed by assuming that only geminate and nearest neighbor e-h pairs are dipole coupled to  $S_o$ . Since  $S_1$  is approximately an all-symmetric combination of such configurations, the bulk of the spectra density is concentrated in this state. Furthermore, the  $S_o \rightarrow S_1$  vibronic band is peaked in the  $0 \rightarrow 1$  C=C stretching feature in agreement with the experimental spectra. Vibronic structure from librations is smeared and produces spectral broadening proportional to Huang-Rhys factors times phonon frequencies. The low-frequency coupling also determines the  $\approx 0.15\text{eV}$  Stokes shift of the  $0 \rightarrow 0$  C=C stretch feature from the adiabatic origin of  $S_1$  at 2.34eV.

## C. Relaxation dynamics

Separated CT states are not eigenstates of the diabatic Hamiltonian and will evolve in time according to the time-dependent Schrödinger equation. Unfortunately, a complete description of the vibronic dynamics is unfeasible due to the enormous size of the state-space. However, we can consider the phonons as a dissipative finite-temperature bath for the electrons and derive reduced equations of motion for the electronic dynamics. For this we turn to the Liouville-von Neumann equation for the

evolution of the electronic density matrix

$$i\hbar\dot{\rho} = [\tilde{H}_{el}, \rho] + \frac{i}{\hbar}\mathcal{R}\rho \quad (11)$$

where the first term represents the unitary evolution of the uncoupled electronic states in the diabatic representation and the second term the non-unitary, dissipative dynamics due to the coupling to the phonon bath. Since the electronic state-space consists of roughly 100 energy levels, we restrict our attention to the population dynamics and decouple populations from coherences according to the Bloch model,

$$\mathcal{R}_{abb} = -k_{ab} + \delta_{ab} \sum_c k_{ac} \quad (12)$$

$$\mathcal{R}_{abab} = \frac{1}{2} \sum_c (k_{ac} - k_{bc}) \quad (13)$$

where  $k_{ab}$  are the rates of elementary interstate transitions. For internal conversions within the diabatic excited states, we assume that the phonons thermalize rapidly on the time-scale of the electronic dynamics such that the one-phonon transitions rates can be determined within the Markov approximation

$$k_{ab} = \pi \sum_{\xi} \frac{(g_{ab\xi}^o)^2}{\hbar\omega_{\xi}} (n_{\xi} + 1)(\Gamma(\omega_{\xi} - \omega_{ab}) - \Gamma(\omega_{\xi} + \omega_{ab})) \quad (14)$$

Here  $n_{\xi}$  is the Bose-Einstein distribution of phonons at  $T = 300\text{K}$  and  $\Gamma$  is the empirical broadening of  $0.01\text{eV}$ . Note that for an elementary  $a \rightarrow b$  population transfer to occur there must a phonon mode  $\omega_{\xi}$  at that transition frequency  $\omega_{ab}$ . Thus, phonon mediated dynamics

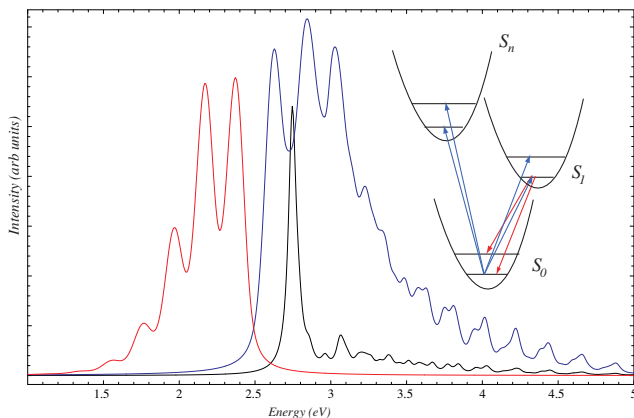


FIG. 2: Computed Condon spectral densities for  $(PPV)_{32}$ . Absorption (blue) and red-shifted emission (red) spectra between the adiabatic ground state and the excited states and the black curve is the oscillator strength for vertical excitation from the ground state. Spectral features correspond to excitation of C=C vibronic stretching modes in the excited state (upon absorption) and in the ground state (upon emission) as detailed in the inset figure.

is restricted to the excited state manifold where the energy level spacing is commensurate with the phonon energies. In contrast, single-photon processes occur across the  $S_0 \rightarrow S_1$  optical gap and the rate of spontaneous emissions is given by

$$k_{a0} = \frac{|\mu_{a0}|^2}{6\epsilon_0\hbar^2} (1 + n(\omega_{a0})) \frac{\hbar\omega_{a0}^3}{2\pi c^3} \quad (15)$$

where  $\mu_{a0}$  are the transition dipoles of the excited singlets. These we can compute directly from the Wannier functions or empirically from the photoluminescence decay rates for a given system. Photon mediated transitions between excited states are highly unlikely due to the  $\omega_{ab}^3$  density factor of the optical field. In essence, so long as the non-equilibrium vibrational dynamics is not a decisive factor, we can use these equations to trace the relaxation of an electronic photo- or charge-transfer excitation from its creation to its decay including photon outflow measured as luminescence.

#### D. Electron-hole capture kinetics

In modeling of e-h capture, propagation starts from the free e-h pair represented by the charge-transfer (CT) configuration with an electron and a hole on the far ends of the polymer chain.

$$|\psi_0\rangle = \left( \begin{array}{cccc} \bar{\downarrow} & \bar{\downarrow} & \cdots & \bar{\downarrow} & \uparrow \\ \downarrow & \uparrow\downarrow & & \uparrow\downarrow & \uparrow\downarrow \end{array} \right) \quad (16)$$

We considered chains with  $n = 2, 4, 8, 16,$  and  $32$  repeat units corresponding to longer and longer polymer chains. The salient data from each of these calculations is presented in Table I. In Fig.1 we show the diabatic density of states (DOS), and the spectral distribution of the starting configuration in S and T state-spaces for a 32 repeat unit chain  $(PPV)_{32}$ . Singlet and triplet populations are also given at an intermediate stage of relaxation at 100ps. In both cases, the system evolves to a metastable superposition state, where half of the density remains locked in CT states ( $S_{CT}$  or  $T_{CT}$ ) above the lowest excitons ( $S_{XT}$  or  $T_{XT}$ ).<sup>21</sup> The branching into CT and XT channels is due to e-h symmetry, which separates excited states into even and odd representations under e-h transposition. Thus, XT states, which are even, are not vibronically coupled to CT states, which are odd. As shown in Fig.3a,  $S_{XT}$  and  $T_{XT}$  are formed at different rates. Whereas  $S_{XT}$ ,  $S_{CT}$  and  $T_{CT}$  show almost parallel population growths, formation of  $T_{XT}$  is far slower.

Assuming that after an initial approach time, the formation of the lowest energy excitons follows first-order kinetics corresponding to the decay of some precursor state, we can fit the population data to an exponential form and obtain the formation rate constants. For the longest chain considered ( $(PPV)_{32}$ ), the formation half-times are  $\tau(S_{XT}) = 17.80\text{ps}$  and  $\tau(T_{XT}) = 174.77\text{ps}$ , i.e.,  $r = 9.8$  corresponding to a 77% EL/PL efficiency, which

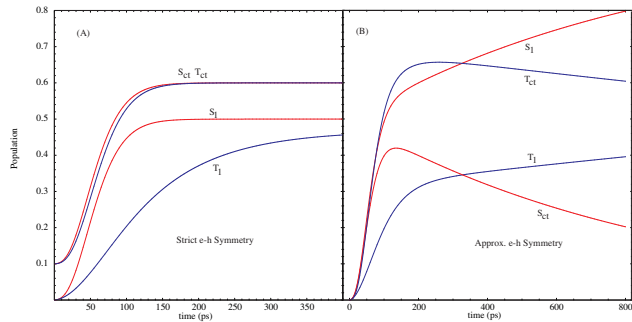


FIG. 3: E-h capture population dynamics of essential states with (A) and without e-h symmetry (B) for 32 unit chain. Singlet populations are in red and triplet populations are in blue.

is systematically higher than observed in both LED<sup>3,5,6</sup> and PADMR<sup>7,8</sup> data, but nevertheless consistent with the observed trend. For physical systems in which disorder limits the effective conjugation length, one might expect the effective conjugation length to be more on the order of 8 to 10 repeat units. For the case at hand, this corresponds to  $r \approx 3$  which is more in line with the experimental observations.<sup>7,8</sup>

In Fig. 4 we plot  $r$  vs  $n$  and recover the nearly linear relation empirically obtained by Wohlgennet et al.<sup>8</sup> for a wide range of conjugated polymer systems. This relation indicates that LED device performance will generally improve if one chooses materials with longer conjugation lengths. One speculative explanation is that the singlet is generally delocalized over the entire conjugation length while the triplet is more tightly bound and more localized. Consequently, increasing  $n$  will accentuate the differences between these two states. The singlet/triplet energy difference  $E_s - E_t$  provides one good measure of the difference between the two states. The splitting is primarily due to exchange correlation energy between the electron and the hole and is in effect a measure of the degree of overlap between the single-particle electron and hole wavefunctions. The more the overlap, the larger the splitting. Plotting the  $r^{-1}(n)$  vs singlet-triplet energy splitting yields Fig. 5 in which we see that

TABLE I: Collected data for various chain lengths (symmetric case).  $\Delta E$  is the splitting between  $S_1$  and  $T_1$ ,  $\varepsilon_S^B$  and  $\varepsilon_T^B$  are the excitonic binding energies,  $\tau_S$  and  $\tau_T$  are the formation half-times ( $\tau = \ln(2)/k$ ),  $r = k_s/k_t$ , and  $\phi = r/(r+3)$  is the electro-luminescent efficiency.

$n$	$\Delta E$ (eV)	$\varepsilon_S^B$	$\varepsilon_T^B$	$\tau_S$ (ps)	$\tau_T$ (ps)	$r$	$\phi$
2	1.552	1.09	2.05	29.35	20.49	0.70	0.19
4	1.309	0.57	1.58	23.08	30.48	1.32	0.31
8	1.199	0.41	1.36	18.88	49.83	2.65	0.47
16	1.174	0.32	1.33	17.12	60.93	3.56	0.54
32	1.146	0.30	1.32	17.80	174.77	9.82	0.77

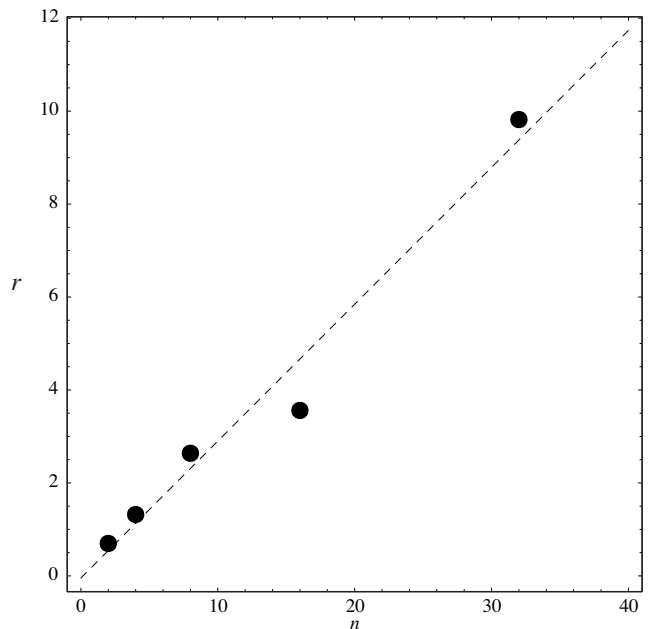


FIG. 4: Linear relation between polymer chain length ( $n$ ) and the rate-constant ratios,  $r(n)$  for singlet and triplet cases. Dashed line is a linear fit to guide the eye.

decreasing the correlation energy leads to an increase in  $r(n)$  and that correlation energy generally decreases with increasing conjugation length.

If we write the branching ratio  $r(n)$  in terms of the transition matrix element from some precursive unbound state to the lowest exciton state, then

$$r(n) = \frac{k_T}{k_S} = \frac{|V_S|^2}{\varepsilon_S} \times \frac{\varepsilon_T}{|V_T|^2} \quad (17)$$

where  $V_{S,T}$  is the matrix element coupling the two states and  $\varepsilon_{S,T}^B$  the singlet or triplet binding energies. If the ratio of the matrix elements varies only weakly in  $n$ , then we can approximate

$$r(n) \approx \frac{\varepsilon_T^B}{\varepsilon_S^B} = R^{-1}. \quad (18)$$

Using the density of states we compute for each chain, we can define the binding energy for the singlet and triplet states as the energy difference between the lowest lying excitonic bound state,  $\varepsilon_{XT}$  and the bottom of the continuum of unbound states lying above the highest lying excitonic state,  $\varepsilon_{CT}$ . In Fig 1 these can be identified by the position of the two peaks (in red) representing the time-evolved population densities and are tabulated in Tab. 1. In Fig. 6 we plot  $r^{-1}(n)$  vs.  $R(n)$  and obtain nearly linear correlation between the two quantities.

Thus, the intrinsic distinction between S and T e-h captures is readily understood in terms of different exciton binding energies<sup>13</sup>. In general, the binding energies for both the singlet and triplet decrease with increasing chain length. However, the difference between the

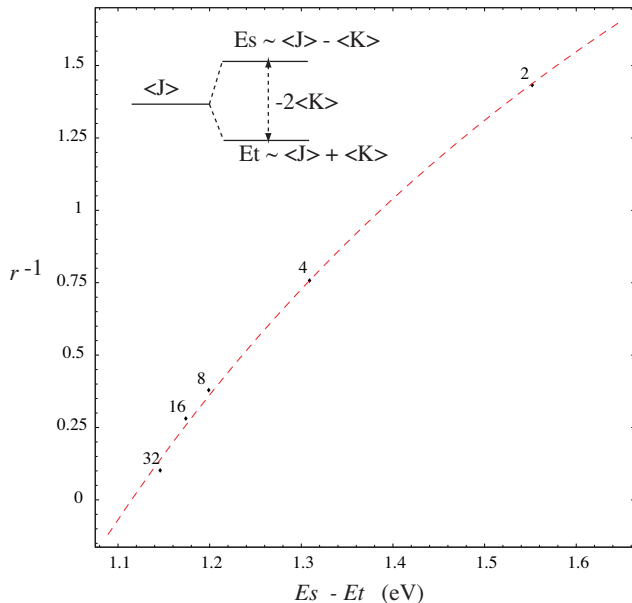


FIG. 5:  $r^{-1}$  vs. e-h correlation energy. Chain length  $n$  is indicated by each point. As indicated by the inset, the singlet/triplet gap is related to the electron/hole exchange energy. Corresponding chain length is indicated by each point. Red dashed curve is a fit to  $a/r$ .

singlet and triplet binding energies remains almost constant at roughly 1 eV for all chain lengths. As seen for the longest chain considered in Fig.1, the singlet excitonic band  $S_{XT}$  nearly overlaps with the charge-transfer band  $S_{CT}$ , whereas in the case of the triplet exciton,  $T_1$  lies at the bottom of a separate band of bound e-h pairs, 1.32eV below the CT continuum. Thus  $T_{XT}$  formation requires on average a longer sequence of vibron-mediated transitions, each falling into the phonon frequency range.<sup>11,12</sup> On the other hand, the singlet binding energy ranges from 1eV (for  $n = 2$ ) to 0.3 eV (for  $n = 32$ ) requiring the excitation of significantly fewer phonons to relax from the lowest unbound singlet to the lowest bound singlet.

### E. Breaking e/h symmetry

The higher efficiency of S recombination becomes more apparent when e-h symmetry is lifted. We slightly broaden the conduction band and squeeze the valence band, so that  $f/\bar{f} = -1.1$ . The small e-h asymmetry changes negligibly the electronic spectrum, but opens a weak vibronic channel for CT $\rightarrow$ XT internal conversions. The resulting population dynamics are shown in Fig.3b. Here we see a fast build-up of low-lying XT and CT states in the first 100 to 200ps, followed by a slow conversion of CT states into excitons. The initial dynamics occurs approximately without e-h parity crossovers and the for-

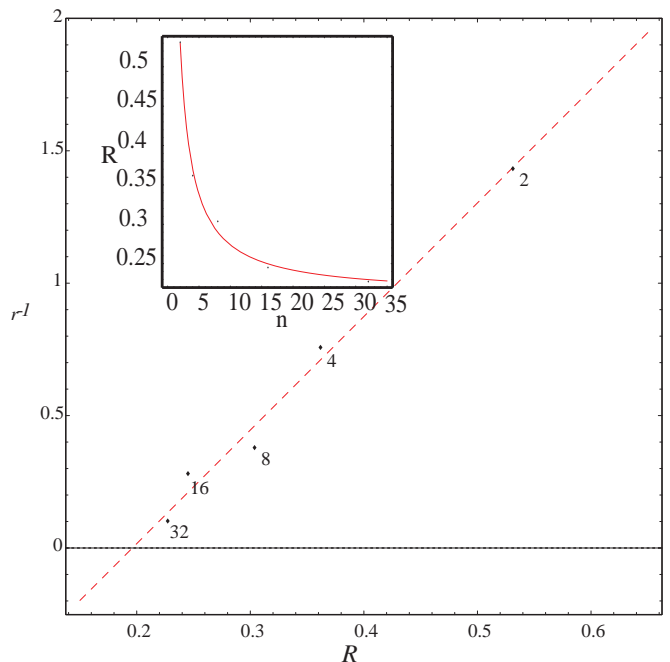


FIG. 6:  $r^{-1}$  vs. the ratio of the exciton binding energies ( $R = \epsilon_S^B/\epsilon_T^B$ ) for various chain lengths. Dashed line is a linear fit to the data. Inset figure shows the variation of  $R$  with chain length.

mation rates of low-lying XT and CT singlets and triplets are about the same as in the symmetric case. However, the triplet XT to CT branching ratio decreases drastically to about 1:2 and suppresses the formation of  $T_{XT}$ . Moreover, subsequent  $T_{CT} \rightarrow T_{XT}$  relaxation is very slow due to the large binding energy of triplet excitons and the low density of states between  $T_{CT}$  and  $T_{XT}$ . Thus  $T_{XT}$  population reaches only 40% after 800ps propagation. In contrast,  $S_{XT}$  is slightly favored over  $S_{CT}$  in the initial capture, and further  $S_{CT} \rightarrow S_{XT}$  conversion occurs on a time scale of about 800ps.

Note as well that  $S_{CT}$  and  $T_{CT}$  are very close in energy because of the lack of appreciable exchange between separated electrons and holes. Hence, intersystem  $S \rightarrow T$  crossing of long-lived CT states due to spin-orbit coupling is highly likely to occur prior to final e-h binding.

### III. CONCLUSION

In summary, we have simulated phonon-mediated intrachain e-h recombination in LCPs. The approach allows us to examine EL quantum yield in LCPs further case by case by combining first-principle description with available spectroscopic data. While we focus here on PPV and adjust el-ph coupling to its absorption spectrum, results can be generalized to most nondegenerate polymers. Apart from spin-degeneracy statistics, efficiency of singlet e-h capture outweighs the triplet one as a natural outcome of the higher binding energy of

triplet excitons. For both S and T processes, the relaxation mechanism involves two steps as a result of approximate e-h symmetry. In the initial e-h capture, both low-lying excitons and same-spin CT intermediates are formed. The XT to CT branching ratio may vary, but is inevitably more favorable for singlet excitons than for triplet ones simply due to energetics. Relaxing to the higher lying singlet exciton requires fewer elementary relaxation steps than the lower lying triplet exciton. Subsequent conversion of CT states into excitons is forbidden by e-h symmetry and occurs on a much slower time scale. The weak e-h asymmetry of real conjugated systems fa-

vors again the singlet  $CT \rightarrow XT$  relaxation by a factor, commensurate with the ratio of T to S exciton binding energies.

### Acknowledgments

This work was funded by the National Science Foundation (CAREER Award) and the Robert A. Welch Foundation.

---

\* email:bittner@uh.edu

- <sup>1</sup> J. H. Burroughes et al., Nature **347**, 539 (1990).
- <sup>2</sup> Y. Cao et al., Nature **397**, 414 (1999).
- <sup>3</sup> R. H. Friend et al., Nature **397**, 121 (1999).
- <sup>4</sup> J. S. Wilson, A. S. Dhoot, and A. J. A. B. Seeley, M. S. Khan, A. Köhler, and R. H. Friend, Nature **413**, 828 (2001).
- <sup>5</sup> J. S. Kim et al., J. Appl. Phys. **88**, 1073 (2000).
- <sup>6</sup> M. A. Baldo, D. F. O'Brian, M. E. Thompson, and S. R. Forrest, Phys. Rev. B **60**, 14422 (1999).
- <sup>7</sup> M. Wohlgenannt, Kunj Tandon, S. Mazumdar, S. Ramasesha, and Z. V. Vardeny, Nature **409**, 494 (2001).
- <sup>8</sup> M. Wohlgenannt, X. M. Jiang, Z. V. Vardeny, and R. A. J. Janssen, Phys. Rev. Lett. **88**, 197401 (2002)
- <sup>9</sup> Z. Shuai, D. Beljonne, R. J. Silbey, and J. L. Bredas, Phys. Rev. Lett. **84**, 131 (2000).
- <sup>10</sup> A. Ye, Z. Shuai, and J. L. Bredas, Phys. Rev. B **65**, 5208 (2002).
- <sup>11</sup> M. Kobrak and E. R. Bittner, Phys. Rev. B **62**, 11473 (2000).
- <sup>12</sup> E. R. Bittner and M. N. Kobrak, Synth. Metals **121**, 1635 (2001).
- <sup>13</sup> J. L. Bredas, J. Cornil, and A. J. Heeger, Adv. Mater. **8**, 447 (1996); J. L. Bredas et al., Acc. Chem. Res. **32**, 267 (1999).
- <sup>14</sup> A. L. Burin and M. A. Ratner, J. Chem. Phys. **109**, 6092 (1998).
- <sup>15</sup> D. Mukhopadhyay, G. W. Hayden, and Z. G. Soos, Phys. Rev. B **51**, 9476 (1995); M. Chandross, Y. Shimoi, and S. Mazumdar, Phys. Rev. B **59**, 4822 (1999).
- <sup>16</sup> P. Karadakov, J. L. Calais, and J. Delhalle, J. Chem. Phys. **94**, 8520 (1991).
- <sup>17</sup> Superscript 0 applies to quantities, taken at ground-state equilibrium, e.g.  $q_\mu = 0$ .
- <sup>18</sup> T. W. Hagler, K. Packbaz, and A. J. Heeger, Phys. Rev. B **49**, 10968 (1994); K. Pichler et al., J. Phys. Cond. Mat. **5**, (1993) 7155; J. Cornil et al., Chem. Phys. Lett. **278**, 139 (1997).
- <sup>19</sup> S. Karabunarliev et al., J. Chem. Phys. **113**, 11372 (2000); 114, 5863 (2001).
- <sup>20</sup> For a recent review see: V. May and O. Khn, Charge and Energy Transfer Dynamics in Molecular Systems (Wiley-VCH, Berlin, 2000).
- <sup>21</sup> By  $S_{XT}$  we mean  $S_1$  and the several other thermally populated singlets above it. Similarly for  $T_{XT}$ ,  $S_{CT}$ , and  $T_{CT}$ .